C. Christopoulos, J. F. Dawson, L. Dawson, I. D. Flintoft, O. Hassan, A. C. Marvin, K. Morgan, P. Sewell, C. J. Smartt and Z. Q. Xie, "Characterization and modelling of electromagnetic interactions in aircraft", Proceedings of the Institution of Mechanical Engineers, Part G: Journal of Aerospace Engineering April 1, 2010 224: 449-458, doi: 10.1243/09544100JAERO567

Keywords: electromagnetic design, electromagnetic compatibility, modelling and simulation, electromagnetic properties of materials, multi-scale techniques

URL: http://pig.sagepub.com/content/224/4/449.abstract

CHARACTERIZATION AND MODELLING OF ELECTROMAGNETIC INTERACTIONS IN AIRCRAFT

C. Christopoulos[1], J. F. Dawson[2], L. Dawson[2], I. D. Flintoft[2], O. Hassan[3], A. C. Marvin[2], K. Morgan[3], P. Sewell[1], C. J. Smartt[1], Z. Q. Xie[3].

[1] George Green Institute for Electromagnetics Research, University of Nottingham, Nottingham, NG7 2RD.
[2] Department of Electronics, University of York, Heslington, York, YO10 5DD.
[3]Civil and Computational Engineering Centre, School of Engineering, Swansea University, Swansea, SA2 8PP.

Abstract: This paper describes the development of modelling techniques and simulation tools for the electromagnetic analysis of aircraft. It is shown that hybrid solvers and multi-scale techniques can be used effectively to analyse the electromagnetic response of aircraft. The importance of supplementing models with appropriate measurement and characterization techniques for parameter extraction and for validation is also demonstrated.

Keywords: electromagnetic design, electromagnetic compatibility, modelling and simulation, electromagnetic properties of materials, multi-scale techniques

Introduction

Current developments in aircraft manufacture are driven by several interlinked requirements foremost among these being the need to reduce weight and therefore save fuel and ameliorate the environmental impact of flying. This means that lighter materials are used based on carbon fibre composites (CFCs) which have exceptional mechanical strength and low weight. This development causes several problems:

i. Such materials have low electrical conductivity, may be anisotropic due to the layered structure of CFCs, and in electromagnetic terms they are not as effective as Aluminium in providing electromagnetic shielding. Electromagnetic (EM) radiation may escape the confines of the aircraft and thus cause interference to other users, or, in the case of military aircraft facilitate its detection.

ii. All aircraft and in particular military aircraft fly in all weather conditions and thus are subject to lightning strikes. Very steep fronted current pulses (risetimes in the order of micro-seconds) of peak amplitudes of several tens of thousands of amps are thus injected at attachment points on the skin of the aircraft. An all aluminium skin is a relatively uniform and isotropic medium and thus the current flow is relatively easy to predict although many difficulties still exist in current flow at joints and rivets. These currents may cause electromagnetic interference (EMI) with safety critical electrical systems inside the aircraft (indirect effects), and/or cause local melting, ruptures and/or fuel ignition (direct effects). Both of these mechanisms have potentially catastrophic effects. CFCs because of their structure and electrical properties make it difficult to predict lightning current flow and interactions with other aircraft systems.

In addition to the innovative new materials being introduced to aircraft manufacture, new configurations are being considered to distribute power for actuation and control. The tendency is to

increase the proportion of electrical power in commercial aircraft to more than 1MW, which is well above its current value, enabling the removal of hydraulic and pneumatic power. It is perceived that this will reduce weight, increase flexibility and redundancy in distribution, so that manufacturing costs and fuel burn will reduce. The consequences of this are that:

i. The potential for EMI is now increased as very large electrical loads are supplied throughout the aircraft. Power electronics techniques are used to supply variable speed drives. This means that power signals are no longer dc or harmonic ac but chopped waveforms with sharp edges containing substantial energy in high order harmonics of the power frequency. Similarly, switched-mode power supplies, which are used in preference to transformer based supplies, use switching frequencies as high as 1MHz, and also contribute energy at higher harmonics (i.e. as high as 30MHz). High frequency signals are capable of coupling more easily to other systems through stray capacitances (Cdv/dt), and/or stray mutual inductances (Mdi/dt). We see that the strength of coupling depends on the rate-of-change and the frequency. Short pulse transition times (i.e. strong coupling) indicates the presence of substantial energy over a wide frequency band.

ii. Not withstanding the benefits of electrical power transmission, it has to be recognised that electrical power distribution at power levels in the MW range co-exists with the low power level signals used for communications, actuation, control, and sensing. The fly-by-wire aircraft is already a reality. The co-existence of high- and low-level signals in close proximity has the potential to cause electromagnetic compatibility (EMC) problems.

It is an interesting statistic of modern aircraft technology that the electrical wiring necessary to operate a typical wide-body passenger jet is 240km long and 17km is required in a modern military fighter aircraft **[1]**. The weight, the complexity of wiring and its repair and maintenance are significant overheads which could be reduced if at least some of the wiring was replaced by wireless connections. The issues to be considered here include:

i. Reduced electrical shielding and high-frequency EMI with this wiring system, and the elimination of the risk of EMC failure, means that the interaction with a more hostile EM environment has to be understood and designed in from the very beginning, to avoid problems at prototype stage when rectification is extremely costly.

ii. If some of the wiring is to be replaced by wireless connections, this must be done in such a way that the quality of service, and the reliability of wireless operated systems is extremely high. This must certainly be higher than that available to mobile phone or Bluetooth users. It is, therefore, necessary to understand and design HF signal propagation inside the complex resonant and multipath environment of a modern aircraft.

The list above, which is not exhaustive, identifies the need for a general EM modelling methodology and computer tools that in the hands of a designer, permit an early stage evaluation of the potential for EMC and lightning problems and helps to identify remedies and optimum solutions. Such a set of tools will substantially de-risk the EM design of aircraft and substantially enhance survivability in the case of failures and interference. It cannot be emphasized enough that the availability of such tools is imperative, if the proposed new technologies are to find acceptance, and if the cost and environmental benefits they promise can be delivered without compromising the extremely high safety and reliability standards rightly expected in the aircraft industry. We also note another potential benefit of such CAD EM tools. It is well known that the costs of demonstrating compliance and certification for EMC for

aircraft are very high. It is hoped that at least some of these tasks could be performed by simulation thus reducing costs and allowing future re-design and the re-fit of new components based on new technologies to be undertaken without a full-scale experimental compliance campaign. It is not suggested, nor is it desirable or realistic, that simulation will completely replace measurement and testing. Rather, it could offer a complementary approach to reduce costs and enhance confidence in the design process. With proper CAD tool validation this is a realistic prospect.

This paper describes results from a research project funded by EPSRC and BAES aimed at making a substantial contribution in this area. It involved three Universities (Nottingham, Swansea, and York) and lasted three years. One full-time researcher was engaged on this work in each of the three Universities. Close collaboration was maintained throughout and substantial interactions took place so that no sharp boundaries existed between the work of each of the partners. However, as an indication of the main themes pursued by the partners, we mention the work at Swansea on the core solver, at York on materials, feature characterization and validation, and at Nottingham on multiscale and materials modelling. These themes are described in more detail in the following sections.

Simulation Software Developments

The simulation software developments were undertaken within the computer code HY3D. This is a hybrid time domain volume based method for the solution of Maxwell's equations. Although solution techniques based upon the use of integral equations are often the best approach for problems that just involve wave scattering **[2]**, a volume based method can be viewed as offering many advantages when a wider range of electromagnetic applications needs to be considered **[3]**. The finite difference time domain (FDTD) approach **[4]** is a popular method for solving high frequency electromagnetic problems on structured cartesian meshes, because of its accuracy characteristics, low operation count and low storage requirements. Unstructured meshes are frequently better suited for practical applications, but progress in developing an unstructured mesh equivalent to the FDTD scheme has proved to be slow **[5]**.

Low order time domain unstructured mesh based solution algorithms can be implemented in a straightforward fashion, but a major computational resource is then required to accurately simulate wave propagation over a significant number of wavelengths. To reduce the computational requirements, while maintaining geometrical flexibility, hybrid solution procedures have been proposed **[6, 7]**, in which the computational domain is represented by an overlapping combination of structured and unstructured meshes. HY3D employs a hybrid solution procedure which couples an extension of an explicit finite element time domain approach (FETD) **[8]** with the FDTD method. Any far field boundary condition is handled by surrounding a truncated physical domain with an artificial perfectly matched layer (PML) **[9]**. An unstructured tetrahedral mesh is used to represent any materials and the immediately adjacent free space region. The remainder of the free space region and the PML are represented by a cartesian mesh **[10]**. In this way, geometric flexibility is maintained, while reducing the computational penalty associated with the unstructured mesh approach. Constraints, imposed by geometric complexity, may result in the generation of unstructured meshes containing elements of a size significantly smaller than would normally be required for accurate wave propagation. Such elements place a severe limitation on the size of the time step that can be used with an explicit scheme and this results in a corresponding increase in the CPU time. To alleviate this problem, an implicit/explicit version of the FETD scheme was introduced, for use in the unstructured mesh region. The implicit scheme is used to advance the solution locally in regions containing the small elements, while the original explicit scheme is used for the remainder of the unstructured mesh.

To enable appropriate transfer of information between the two solution approaches, an overlapping mesh technique is employed. The mesh that is designed to accomplish this may be regarded as being constructed of three distinct regions. The first region is an assembly of unstructured tetrahedral elements in the vicinity of any materials; the second region consists of an assembly of structured hexahedral cartesian elements, extending to the far field; the third region consists of a structured assembly of hexahedral elements that are each subdivided into six tetrahedral elements. Elements in the third region are employed to enable the transfer of information between the FETD algorithm and the FDTD algorithm to be accomplished in a convenient manner. The mesh is generated in three stages. In the first stage, an unstructured triangulation of any body surface is performed. This is used to construct, in a second stage, a staircase shaped surface lying close to the body and completely enclosing it. The region between this staircase shaped surface and the far field boundary is then discretised to produce the hexahedral cartesian grid and the structured tetrahedral grid. The third stage consists of generating the unstructured grid between the surface triangulation of the body and the staircase surface. The mesh generation process is completed, in a preprocessing phase, by merging the unstructured and structured tetrahedral meshes to form the mesh that is used for the hybrid scheme.

The process of exchanging information between the unstructured and cartesian meshes is simplified by ensuring that the vertices in both meshes coincide exactly in the overlap region. This is achieved by adding structured layers to the unstructured mesh, in which each hexahedron in the corresponding structured mesh is subdivided into six tetrahedral elements. Five such layers are constructed and three of these layers are used to define the overlap region. The variables in the FDTD scheme are stored at staggered locations, while the variables in the FETD scheme are co- located and stored at the vertices. This means that, in the region of overlap, the field components of the two schemes are not available at the same location. When exchange of information is necessary between the meshes, the electric field components for the FETD scheme are evaluated from the corresponding FDTD electric field values by cubic interpolation along the surrounding edges. The magnetic field components for the FETD scheme are located at the centre of the square formed by points at which four corresponding magnetic field components are known in the FDTD scheme. In this case, bi-cubic interpolation is used to transfer the FDTD values to the nodes of the FETD algorithm.

For this solution procedure, accuracy requirements imply that the required mesh size will expand rapidly as the electrical length of interest is increased. The resulting simulations will be computationally demanding and, in this case, the use of parallel computers becomes desirable. The parallel implementation adopted avoids the creation of any global array which can prevent an efficient performance of the algorithm. The generated mesh is first partitioned using the ParMetis library **[11]**. This produces high quality partitions in a fast, robust and parallel manner. The partitioning has to take into account that a staggered scheme is being parallelised and a synchronisation step exists between the different schemes. It is not sufficient to simply sum up the relative times required for each scheme and to compute a partitioning based on this sum. This will lead to some processors having too much work, if the majority of their mesh belongs to one scheme, while others remain idle. This is avoided by using the multi-constraint graph partitioning scheme that minimises edge-cut and ensures that every sub-domain has approximately the same amount of each mesh type. In the parallel implementation of the solution algorithm, elements are owned by only one domain and are not duplicated, while points are owned by one domain and are duplicated. This strategy enables data locality to be achieved during the gather process, from points to elements, and the scatter process, from elements to points, and hence there is no need to communicate. To avoid communication during the interpolation process, the nodes required to perform the interpolation are added to the list of interface nodes and sent to the processor containing the interpolated node. This will ensure that synchronization is only required once per time

step. Parallelization of the implicit procedure can be achieved by assuming that a given number of processors will be used to handle the implicit regions, where the number used is proportional to the total number of implicit elements.

As an example of the performance that can be achieved with HY3D, consider the problem of scattering of a plane single frequency wave by a PEC UAV configuration, of electrical length 25λ. The incident wave propagates along the main axis of the UAV, with the wave impinging directly onto the nose. A wireframe of the UAV and a detail of the discretised surface in the vicinity of the trailing edge is given in Figure 1. The complete mesh consisted of approximately 15.8M tetrahedral elements and around 9M finite difference free space and PML cells. The geometrical form of the trailing edge imposes severe restriction on the size of the elements in that region, which means that 4797 time steps are required to perform a complete cycle using the explicit scheme. The corresponding CPU time needed to advance the solution for one cycle is 50 minutes on 128 IBM processors. Using the implicit/explicit version of the scheme and imposing the requirement of 200 steps per cycle, 850 points are advanced implicitly and the CPU time required to compute one cycle reduces, by a factor of 22, to 2.2 minutes. This means that the time required to complete the calculation is reduced from one day to one hour. A view of the computed distribution of contours of a component of the electric field on the UAV surface is shown in Figure 2.

Incorporating Sub-scale Features

Coupling paths for electromagnetic threats into an airframe may be through antennas (front door coupling), via apertures such as gaps, slots or joints and we must also consider diffusive penetration through materials for low frequency lightning threats (Figure. 3). Once inside the airframe the electromagnetic energy is free to couple onto interconnecting cables and hence into aircraft systems where it may result in disruption or damage to the onboard systems.

A common feature of the coupling paths for the electromagnetic energy outlined above is that they involve features which are small on the scale of the aircraft as a whole. The modelling of such small features on the scale of a full aircraft is very challenging as explicitly meshing the geometry is not feasible **[12]**. An important aspect of the development of HY3D as a practical electromagnetic threat prediction tool is therefore the ability to model features which are significantly smaller than the mesh dimension.

Modelling the pickup of the electromagnetic energy on the cables connecting the on-board systems is vital in order to assess the threat to the aircraft. The fields around cables cannot be represented using the normal linear, continuous finite element shape functions. In the HY3D code we introduce shape functions specifically for wires which incorporate the known 1/r dependence of the radial electric field and circumferential magnetic field close to a cylindrical wire. Introducing these additional shape functions into the finite element analysis leads, after some manipulation and simplification, to an algorithm in which a system of equations describes the propagation of signals on the cables with a source term which represents coupling of energy from the external illuminating field onto the wires. An additional source term is introduced into the field update which represents the radiation of energy from the wire into the field. The resulting approach in which the field update and the wire update are separated but coupled through source terms is similar in concept to the Holland and Simpson wire model for the FDTD method **[13]**. The HY3D wire model is readily generalised to multi-conductor cable bundles and allows the currents at the cable terminations to be calculated, i.e. those injected into the aircraft systems.

Unlike the case of wires where the field close to a cylindrical conductor has a known distribution, in more geometrically complex situations such as a surface containing apertures, slots or joints the local field distribution is not necessarily known. Models of such features for implementation in the HY3D code may be constructed from a characterisation of the scattering (S) parameters of the feature, i.e. how waves are reflected from and transmitted through the feature. This approach is in common with the model for thin material layers described in the next section below. The implementation of the model uses an impedance representation which relates the tangential electric and magnetic fields either side of the interface containing the feature **[14]**. This defines a boundary condition which is applied on surfaces in the HY3D code. The impedance (Z) parameters are readily calculated from the scattering parameters **[15]**.

The scattering parameters may be found from an appropriate measurement of a sample containing the feature, or alternatively a detailed numerical analysis of the isolated feature can lead to the impedance representation directly as illustrated below for the example of an overlap joint (figure 4).

The joint is illuminated by a pulse plane wave, during the analysis tangential electric and magnetic fields either side of the slot are recorded. These time domain fields are then Fourier transformed and used to derive an impedance boundary representation of the joint in the frequency domain.

The parameters of the impedance boundary model for a slot, in common with the models which are derived for materials and thin layers, are frequency dependent. In order to incorporate these frequency dependent properties into the time domain code HY3D an approach based on digital filters (effectively recursive convolution) is utilized **[16]**. When using this approach it is convenient to express the frequency dependence of model parameters as a rational function in complex frequency (equation 1)

$$f(j\omega) = \frac{a_0 + a_1(j\omega) + a_2(j\omega)^2 + \cdots}{b_0 + b_1(j\omega) + b_2(j\omega)^2 + \cdots} \qquad (1)$$

where the order of the expansion and the coefficients are chosen so as to best fit the function to be represented **[17]**. From this rational function a digital filter coefficients may be derived which are then used in the update of the boundary conditions in the finite element update **[18]**.

Material Measurements and Models

Should we include something about bulk dielectric material models as well as boundary conditions for CFC? (CJS)

Within the HY3D code a metal surface can be modeled using PEC boundaries while other types of material surfaces can be represented using frequency dependent impedance boundaries. The reflection coefficient of the material boundaries determines the wall losses on the inside of an airframe and therefore impacts on the quality factor of the cavities inside the aircraft. The transmission coefficients determine the ingress of energy into the airframe and therefore and contribute to the immunity of the aircraft to external EM threats. Accurate knowledge of the frequency dependent characteristics of non-metallic boundaries is therefore an important requirement for EM analysis.

Models for the impedance matrix of a material can be derived in a number of ways. Very high-resolution FDTD simulations can be used if the structure of the material is known accurately. Analytical models can

also be developed - a multi-layer model for a simplified carbon-fiber composite (CFC) structure was recently derived in **[19]**. The internal structure of modern composite materials is however very complex and subject to manufacturing variations so it is currently very difficult to derive accurate impedance boundary models from theoretical analysis alone. Incorporation of measurement data into the material models is therefore essential for accurate EM analysis.

If full magnitude and phase information for the transmission and reflection coefficients of a material were available then a direct approach to fitting the measurement data using the vector fitting technique would be feasible. However, in practice it is usually impossible to achieve this due to the limitations of the available measurement techniques. For example, many samples of interest, such as CFC laminates and perforated metal plate, have very high reflectivity that is difficult to measure accurately. Four different measurement techniques that can provide partial information on the shielding characteristics of materials have been considered and are summarised in Table 1. Priority has been given the shielding measurement techniques since for the simulation of system immunity the transmission through the material is the critical factor.

Table 1: Capabilities of material measurement techniques.

Technique	**Reflectiion (R) and/or Transmission (T)**	**Phase**	**Polarisation**	**Angle of Incidence**	**Frequency Range (GHz)**	**Dynamic Range (dB)**
ASTM D4935 [20]	R/T	Yes	Averaged	Normal	DC-2	100
NRC [21]	T	No	Averaged	Averaged	>1	70
Anisotropic Cells [22]	T	Yes?	Yes	Normal	0.5-2	80
Absorber System [23]	T	Yes?	Yes	Normal	>1	80

The shielding effectiveness (SE) of a 0.5 mm thick aerospace CFC measured using three different techniques is shown in Figure 5. For this material the agreement between all three techniques is very good, though there is some evidence that the ASTM cell is showing a different trend at high frequencies. The measured SE is compared to a simple analytical model for the SE of a homogeneous resistive material, for which the full impedance matrix can be determined analytically **[24]**, with two different sets of parameters. Using the physical thickness of the sample, 0.50mm, the analytical model can be fitted to the low frequency SE yielding an effective conductivity of 3.4 kS/m. Alternatively, allowing the thickness in the analytical model to be a free parameter a better overall fit the measured data can be obtained with a thickness of 1.50 mm and conductivity of 1.1 kS/m. Neither of these analytic models is actually a good fit to the measured data. This indicates the importance of the ability to use measured material properties in the EM analysis.

In order to include measurement data like Figure 5 in HY3D the magnitude and phase of both transmission (SE) and reflection coefficients must be known or inferred. The reflection coefficient, which is difficult to measure, can be estimated from the SE using energy conservation while the phase can be approximated using, for example, the resistive sheet model. Combining these approaches a physically realizable response for the material, incorporating the measured SE, can be generated and fitted to a digital filter representation of the material boundary.

Code Validation

Validation of some features of the code, such as material and thin layer models may be achieved by comparison of HY3D predictions with analytic solutions. Spherical geometries are especially useful as the fields may be expressed as an expansion in terms of spherical Bessel functions. This enables validation for problems with multiple materials, including impedance boundary layers **[25]**. The implementation of the CFC model is tested in this way as shown in Figure 6. The impedance parameters of a physical model of the CFC (Figure 6a) are calculated as a function of frequency and a frequency dependent impedance boundary model derived (Figure 6b). This impedance boundary is applied to a spherical shell and illuminated with a Gaussian pulse. The internal electric field at the centre of the sphere is used as the basis for comparison with an analytic solution for this problem and the agreement in Figure 6c is seen to be extremely good.

Fine feature models may be validated against predicted solutions on a very fine grid, in which the feature may be meshed explicitly. Figure 7a shows the impedance parameter z_{11} for the overlap joint when illuminated by a wave with the electric field polarised in the plane of the slot (TE). Once the impedance matrix for the slot is derived, its properties are then applied on to the enclosure boundary at the position of the joint in the computational mesh, so that the behaviour of the slot is incorporated into the model. Time domain fields inside a 2 dimensional cavity modelled using the impedance boundary approach and a fine grid model in which the slot is explicitly meshed are shown in Figure 7b. Application of the impedance boundary model for the joint is found to reduce the number of elements in the mesh by a factor of 12 and the runtime is reduced by a factor of 40.

For more complex geometries including wires, slots, joints and apertures, validation against measurement is often the only possibility. If a validation against a measurement is to be attempted then the geometry and materials must be well characterised and a non-invasive measurement technique should be used. We are interested in the coupling of electromagnetic energy onto wires in a resonant environment and the code validation measurements should reflect this. To this end, a resonant box has been constructed. The box contains wires which are connected to ports through the walls of the box. The ports may be connected to load or to a network analyser.

For a validation measurement we require a very well controlled and non-invasive measurement i.e. a measurement in which the measuring equipment will not unduly influence the result. The coupling between the wire ports is used as the basis for comparison in this validation rather than the field inside a cavity as the field measurement would require a field probe to be placed inside the box and this probe could be expected to influence the results.

Unloaded cavities have a very high Q factor determined by wall reflection losses. These losses are very difficult to quantify and therefore difficult to include in a model. In order to control the Q of the cavity, one side of the box is left open. This reduces the Q of the system to a value which is realistic for a loaded cavity such as would be found on an aircraft.

Inset in figure 8 is a photograph of the validation box with the lid reversed to show a monopole connected to one port and a wire loop connecting the other two ports. The measured and predicted coupling between the monopole and a wire port are shown in the figure to be very close over the whole frequency range of the prediction. This gives confidence in the use of the HY3D code as a prediction tool for electromagnetic threat prediction in aircraft.

[Comparision techniques?]

Conclusion

The development of a modelling and simulation technique for the electromagnetic design of aircraft has been described. It has been shown that hybrid modelling techniques can be used effectively to model parts of complex systems in an efficient manner. In addition, multi-scale models are required which permit the embedding of electrically small features into numerical models of electrically large objects. Examples included in this paper have demonstrated how models for joints, apertures and thin wires may be included. Current practice in aircraft manufacture favours the use of composite materials and corresponding material models have also been developed and embedded into large scale numerical simulations. Experimental techniques for obtaining the parameters for such models were also described. Some validation results were provided to demonstrate the accuracy of the models developed. This work is ongoing and aims, eventually, to provide a full capability for the computer-aided electromagnetic design of complex aircraft systems.

Acknowledgements: This work was supported by grants from EPSRC and BAE Systems. We also acknowledge the advice we received from BAE Systems experts throughout the duration of the project and in particular the support from Professor David Rowse.

References:

1. A. A C. Furse, R. Haupt, Down to the Wire, *IEEE Spectrum **38**(2):34-39, 2001*

2. W. C. Chew, Computational electromagnetics: the physics of smooth versus oscillatory fields, *Philosophical Transactions of the Royal Society: Mathematical, Physical and Engineering Sciences* **362**:579−602, 2004.

3. J. S. Hesthaven and **T. Warburton**, High order nodal discontinuous Galerkin methods for the Maxwell eigenvalue problem, *Philosophical Transactions of the Royal Society: Mathematical, Physical and Engineering Sciences* **362**:493−524, 2004.

4. K. S. Yee, Numerical solution of initial boundary value problems involving Maxwell's equations in isotropic media. *IEEE Transactions on Antennas and Propagation* **14**:302−307, 1966.

5. I. Sazonov, D. Wang, O. Hassan, K. Morgan and **N. P. Weatherill**, A stitching method of unstructured mesh generation for co—volume solution techniques, *Computer Methods in Applied Mechanics and Engineering* **195**:1826−1845, 2006.

6. T. Rylander and **A. Bondeson**, Stable FEM--FDTD hybrid method for Maxwell's equations, *Computer Physics Communications* **125**:75−82, 2000.

7. F. Edelvik and **G. Ledfelt**, A comparison of time−domain hybrid solvers for complex scattering problems, *International Journal of Numerical Modelling: Electronic Networks, Devices and Fields* **15**:475--487. 2002.

8. K. Morgan, O. Hassan, N. E. Pegg and **N. P. Weatherill**, The simulation of electromagnetic scattering in piecewise homogeneous media using unstructured grids, *Computational Mechanics* **25**:438−447, 2000.

9. J. P. Berenger, A perfectly matched layer for free space simulation in finite difference computer codes, *Journal of Computational Physics* **114**:185--200, 1994.

10. M. El Hachemi, O. Hassan, K. Morgan, D. Rowse and **N. Weatherill**, A low order unstructured mesh approach for computational electromagnetics in the time domain, *Philosophical Transactions of The Royal Society: Mathematical, Physical and Engineering Sciences* **363**:445−469, 2004.

11. G. Karypis and **V. Kumar**, Multilevel k-way partitioning scheme for irregular graphs, *Journal of Parallel and Distributed Computing* **48**:96−129, 1998.

12. C Christopoulos. Multi-scale Modelling in Time-Domain Electromagnetics. *Int. J. Electron. Commun. (AEÜ)*, Vol.**57**, No.**2**, pp.100-110, 2003.

13. R. Holland, L. Simpson, Finite-Difference Analysis of EMP Coupling to Thin Struts and Wires. *IEEE Trans EMC,* Volume **23**, no **2**, pp 88 – 97, 1981.

14. T. B. A. Senior, J. L. Volakis, Approximate boundary conditions in electromagnetics. *Institution of Electrical Engineers*, 1995.

15. R. E. Collin, Field Theory of Guided Waves. 2nd Edition. *IEEE Press*, 1991.

16. C. Hulse, Dispersive models for the finite difference time domain method: design, analysis and implementation. *J. Opt. Soc. Am*. Vol. **11,** no**. 6**, pp. 1802-1811, 1994.

17. B. Gustavsen and **A. Semlyen**, Rational approximation of frequency domain responses by vector fitting. *IEEE Trans. Power Delivery*, vol. **14**, no. **3**, pp. 1051-1061, July 1999.

18. J. Paul, V. Podlozny, C. Christopoulos, The Use of Digital Filtering Techniques for the Simulation of Fine Features in EMC Problems Solved in the Time-Domain, *IEEE Trans. On EMC*, Vol.**4**5, No.**2**, pp.238-244, May 2003

19. C. Holloway, M. Sarto and **M. Johansson**, Analyzing carbon-fiber composite materials with equivalent-layer models, *IEEE Trans. Electromag. Compat*., vol. **47**, no. **4,** pp. 833-844, November 2005.

20. ASTM, Standard test method for measuring the electromagnetic shielding effectiveness of planar materials*, American Society for Testing and Materials*, **Standard D4935-99**, 1999.

21. IEC, Testing and measurement techniques - reverberation chamber test methods, *International Electrotechnical Commission*, **Standard 6100-4-21:2003**, 2003.

22. C. L. Holloway, D. A. Hill, J. Ladbury, G. Koepke and **R. Garzia**, Shielding effectiveness measurements of materials using nested reverberation chambers*, IEEE Trans. Electromag. Compat*., vol. **45**, no. **2**, pp. 350-356, May 2003.

23. A. C. Marvin, L. Dawson and **I. D. Flintoft**, A novel contact-less shielding effectiveness measurement technique for planar material samples, in Workshop on EMC Measurements and Test Facilities, *International Symposium on Electromagnetic Compatibility*, EMC Europe 2006, Barcelona, September 2006.

24. J. A. Cole, J. F. Dawson and **S. J. Porter**, A digital filter technique for electromagnetic modelling of thin composite layers in TLM, in *13th Annual Review of Progress in Applied Computational Electromagnetics*, March 1997.

25. G. T. Ruck, D. E. Barrick, W. D. Stuart, C. Kirchbaum, *Radar Cross Section Handbook*, volume **1**, Plenum Press, New York, 1970.

Figure Captions:

Figure 1: Scattering of a plane wave by a PEC UAV configuration: (a) wire frame of the UAV surface; (b) detail of the surface mesh in the vicinity of the trailing edge.

Figure 2: Scattering of a plane wave by a PEC UAV: contours of a component of the electric field on the surface.

Figure 3: Coupling paths for electromagnetic threats to an aircraft, here the Eclipse UAV.
(Photographs supplied by Cranfield University.)

Figure 4:

- Figure 4a. Overlap joint in an enclosure.
- Figure 4b.Enclosure model with impedance boundary.
- Figure 4c. Frame from a detailed analysis of the scattering from the joint which leads to the impedance boundary model.

Figure 5: Shielding effectiveness (inverse transmission coefficient) of a two-layer aerospace CFC laminate measured using different techniques.

Figure 6:

- Figure 6a Shielding effectiveness (inverse transmission coefficient) of a two-layer aerospace CFC laminate measured using different techniques.
- Figure 6b. Calculated Impedance parameters for the physical model and the fitted 6^{th} order impedance boundary model.
- Figure 6c.HY3D prediction and analytic solution for the field at the centre of the CFC spherical shell as a function of time when illuminated by a Gaussian pulse.

Figure 7:

- Figure 7a. Overlap joint impedance, TE polarisaton.
- Figure7b. Cavity Field with explicitly meshed slot (red) and impedance boundary representation (green).

Figure 8: Coupling between monopole and port on the wire: measurement and HY3D result and the box shown inset (with the lid reversed).

(a)

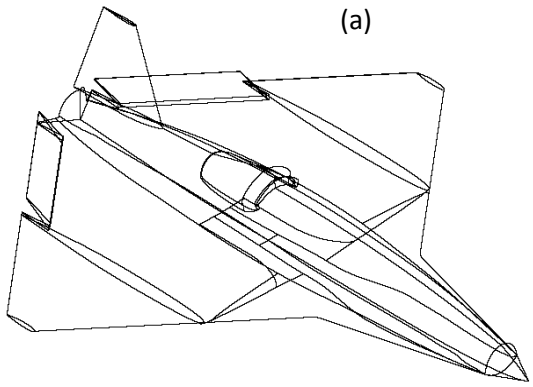

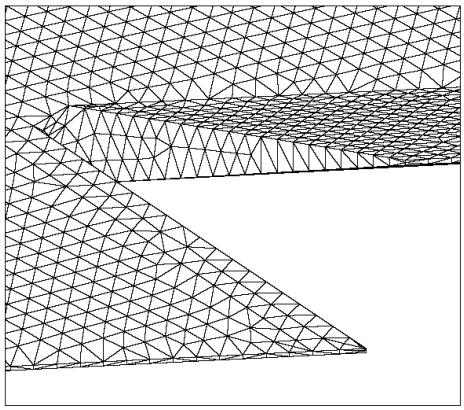

(b)

Figure 1.

Figure 2.

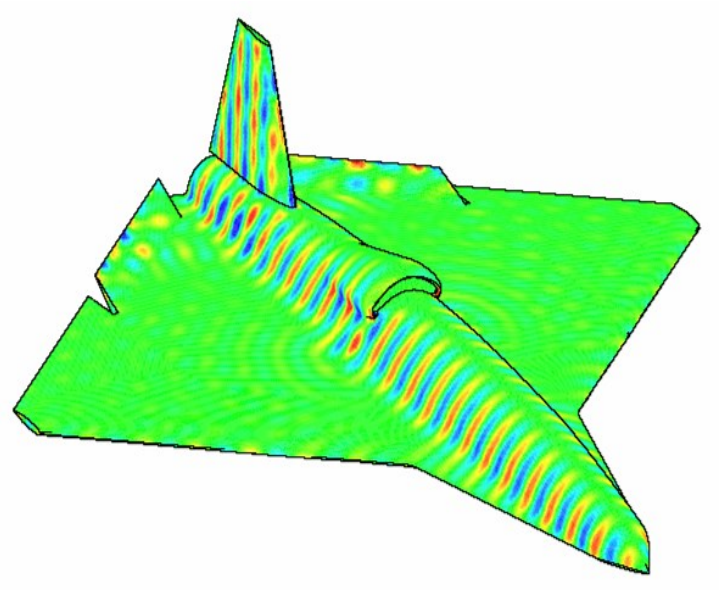

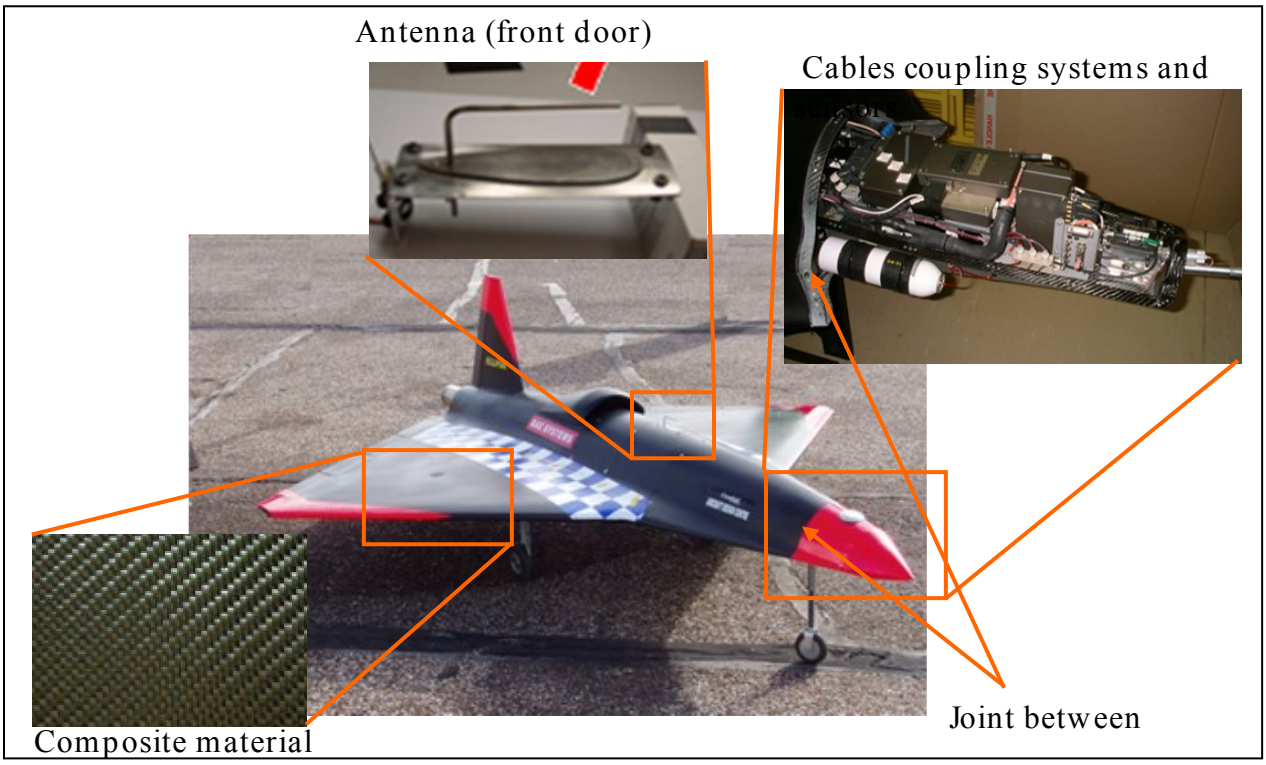
Antenna (front door)
Cables coupling systems and
Joint between
Composite material

Figure 3.

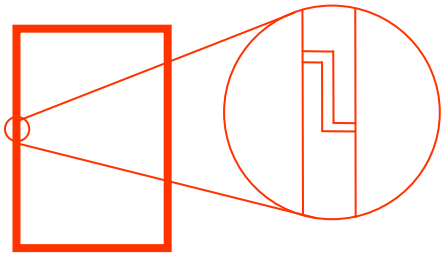

Figure 4a.

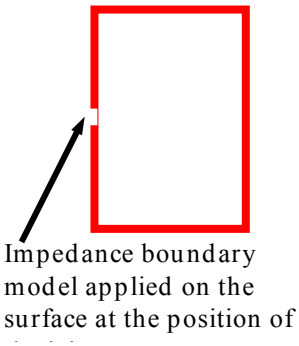

Figure 4b.

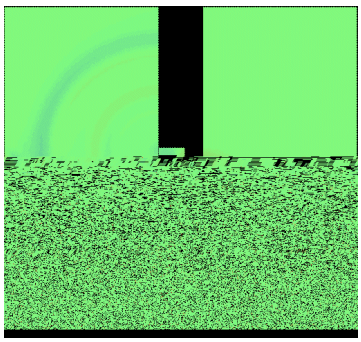

Figure 4c.

Figure 4.

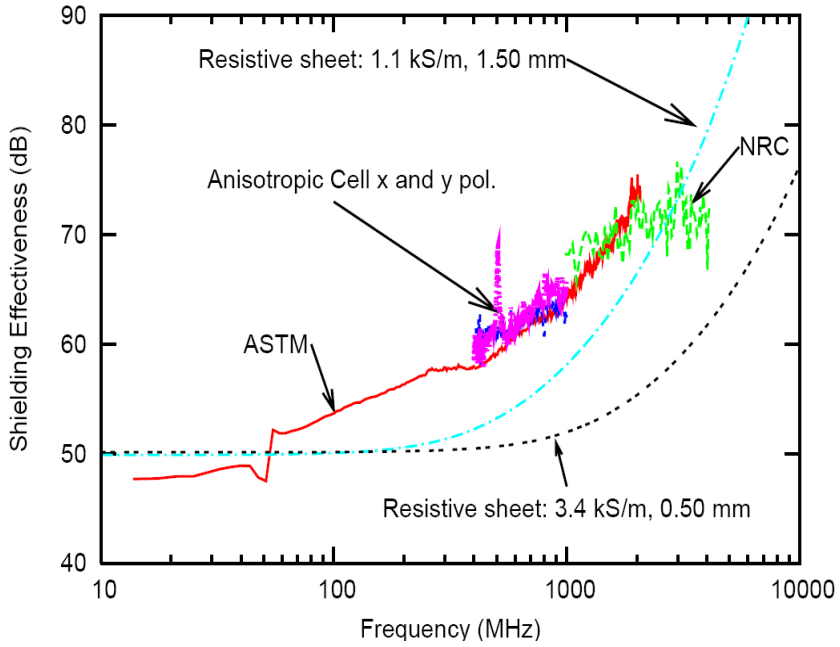
Resistive sheet: 1.1 kS/m, 1.50 mm
NRC
Anisotropic Cell x and y pol.
ASTM
Resistive sheet: 3.4 kS/m, 0.50 mm
Shielding Effectiveness (dB)
Frequency (MHz)
90
80
70
60
50
40
10
100
1000
10000

Figure 5:

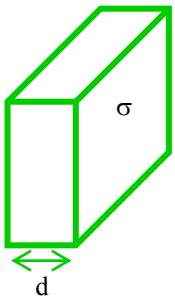

Figure 6a.

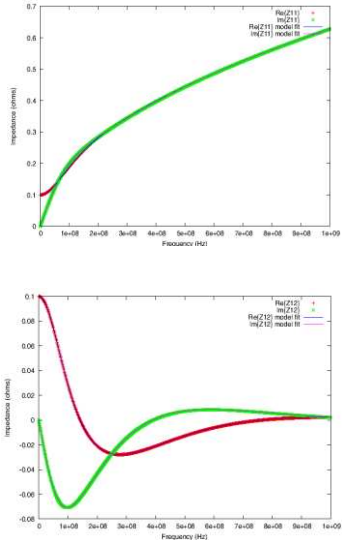

Figure 6b.

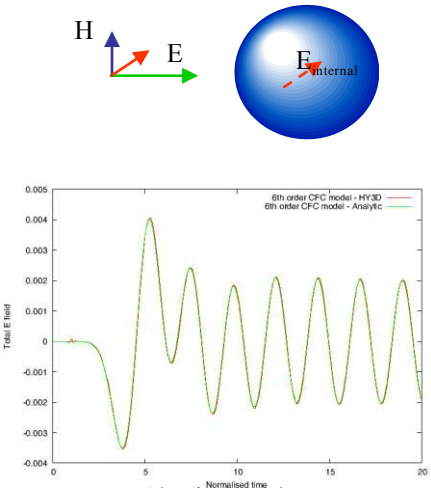

R=1/ σd=0.1Ω/□

Figure 6c.

Figure 6.

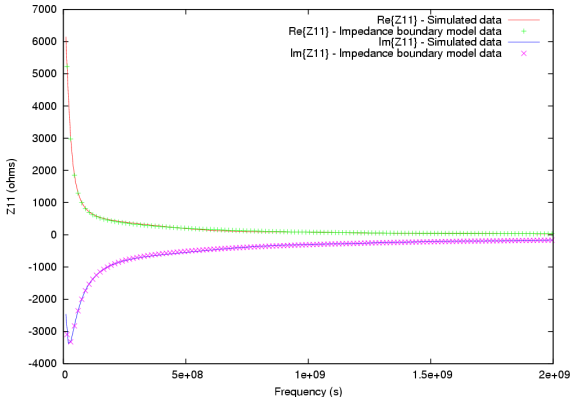

Figure 7a.

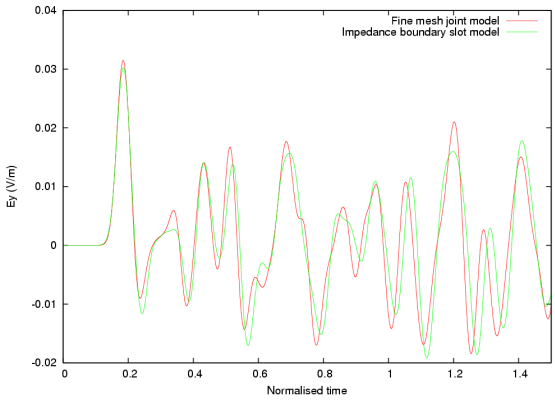

Figure 7b.

Figure 7.

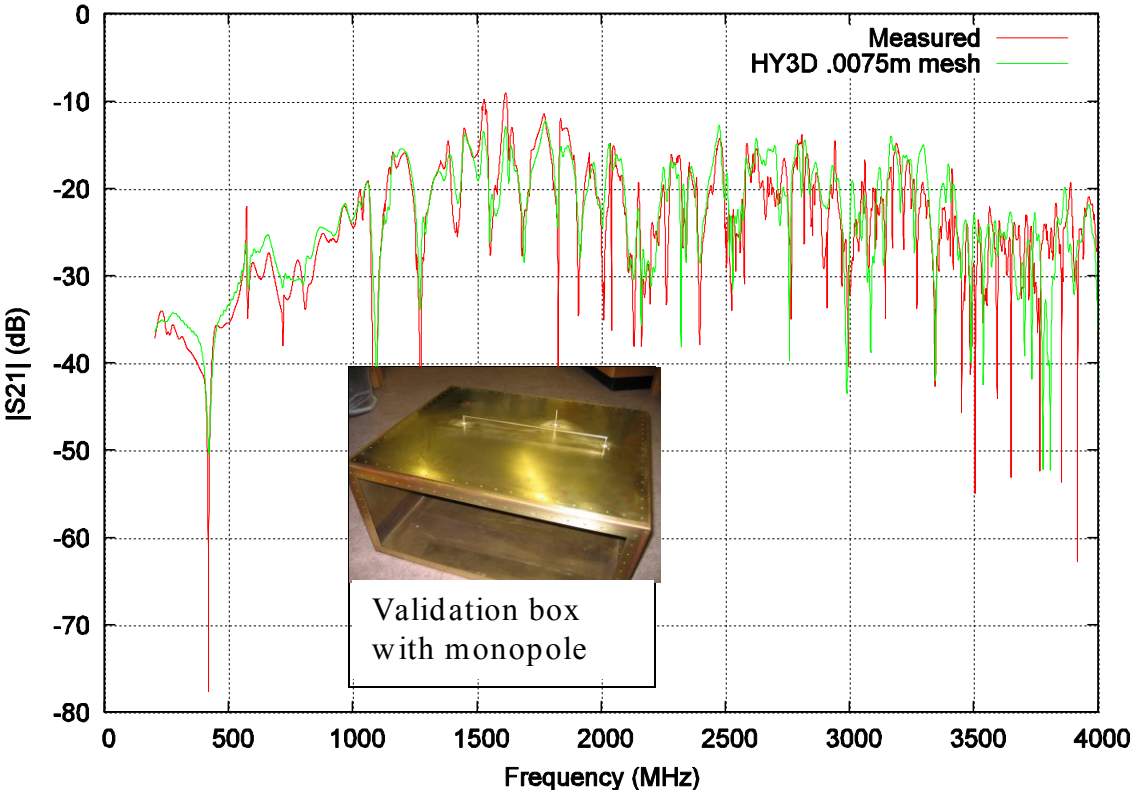
Measured
HY3D .0075m mesh
|S21| (dB)
Frequency (MHz)
0
-10
-20
-30
-40
-50
-60
-70
-80
0
500
1000
1500
2000
2500
3000
3500
4000
Validation box
with monopole

Figure 8.